Maser-beam instability of Bernstein waves

L. F. Ziebell, Peter H. Yoon, and C. S. Wu

Citation: Physics of Plasmas **7**, 4720 (2000); doi: 10.1063/1.1313567
View online: http://dx.doi.org/10.1063/1.1313567
View Table of Contents: http://scitation.aip.org/content/aip/journal/pop/7/11?ver=pdfcov
Published by the AIP Publishing

Maser-beam instability of Bernstein waves

L. F. Ziebell,[a] Peter H. Yoon,[b] and C. S. Wu
Institute for Physical Science and Technology, University of Maryland, College Park, Maryland 20742

(Received 12 June 2000; accepted 3 August 2000)

The present study constitutes a continuation and improvement of the preceding work by Yoon *et al.* [J. Geophys. Res. **104**, 19801 (1999)]. In the present discussion, an instability of Bernstein waves excited by a beam of energetic electrons is investigated. Special attention is paid to the regime where the ratio of plasma frequency, ω_{pe}, to electron gyrofrequency, Ω_e, is sufficiently higher than unity. An approximate but fairly accurate scheme is introduced to deal with the situation dictated by the condition, $\omega_{pe}^2/\Omega_e^2 \gg 1$. The present investigation is motivated by the research in solar radiophysics. However, in this article the emphasis is placed on basic properties of the instability rather than its application. © *2000 American Institute of Physics.* [S1070-664X(00)02811-1]

I. INTRODUCTION

Plasma instabilities associated with a beam of electrons are extensively discussed in the literature. Discussions are usually based upon the model that the beam electrons possess a displaced Maxwellian distribution function[1]

$$f_b(\mathbf{u}) = A \exp[-(\mathbf{u}-\mathbf{u}_b)^2/\alpha_b^2], \tag{1}$$

where $\mathbf{u}=\mathbf{p}/mc$ is the normalized momentum, m and c being the mass of a given particle species, and the speed of light *in vacuo*, respectively, A is an appropriate normalization constant, α_b represents the momentum dispersion, and $\mathbf{u}_b$ is related to the average drift velocity $\mathbf{v}_b$ by $\mathbf{u}_b=(\mathbf{v}_b/c)(1-v_b^2/c^2)^{-1/2}$. Using this model distribution, one can readily show that Langmuir waves are excited, when the beam speed is sufficiently high.

Strictly speaking, however, this model distribution is valid only if the background plasma is quiescent. Thus, it may not be appropriate for the study of plasma processes near the Sun because high level of intrinsic hydromagnetic turbulence exists pervasively in solar-terrestrial environments. One of the consequences is that enhanced hydromagnetic waves can result in pitch-angle scattering of electrons, and such a process can in turn significantly modify the beam electron distribution function. Considering such an effect, it was shown in Ref. 2 that Bernstein waves can also be excited. In the discussion presented in Ref. 2, it is proposed that Eq. (1) be replaced by a model distribution of the form,

$$\begin{aligned} f_b(\mathbf{u}) &= A' g(\mu) \exp[-(u-u_b)^2/\alpha_b^2], \\ g(\mu) &= 1+\tanh[(\mu-1)/\delta], \end{aligned} \tag{2}$$

where A' is the normalization constant, u is the magnitude of the momentum vector, and $\mu=u_\parallel/u$ is the cosine of the momentum space pitch-angle, $u_\parallel$ being the component of the momentum parallel to the ambient magnetic field. In the above, the effects of pitch-angle scattering by low-frequency hydromagnetic waves is implicitly modeled by the parameter δ, which is presumed to be proportional to the level of the turbulence in some unspecified manner. Here we reiterate that the simple Maxwellian beam of the form (1) is stable for Bernstein waves, whereas the modified beam (2) can excite these waves. An explanation of the significance of this work is perhaps in order.

As is well-known, there are two types of waves whose wave vectors lie perpendicular to the ambient magnetic field, namely, the extraordinary and ordinary modes. When thermal effects are ignored, extraordinary mode reduces to fast (X) and slow (Z) modes.[1] In addition to X and Z modes, a thermal plasma can support electrostatic Bernstein waves,[3,4] which can be considered as part of the extraordinary mode in the quasi-electrostatic limit.[2,5,6]

An important point is that there exist numerous ''windows'' at gyroharmonic frequencies via which Bernstein waves can be converted to fast (X) mode. Such a conversion is likely to be a natural consequence of a plasma immersed in a nonuniform magnetic field. From the standpoint of radiophysics, the excitation of Bernstein waves and subsequent linear mode conversion to electromagnetic waves[7] constitute an entirely new mechanism to produce radio emission, which has not been considered before.

In passing, we ought to remark that applications of Bernstein waves for a number of problems concerning laboratory, space, and astrophysical plasmas have been discussed in the literature.[8–22] However, the physical situations considered in these works are different from that of interest to us. We are particularly interested in the situation in which the ratio of plasma to electron gyro-frequencies is much higher than unity, $\omega_{pe}^2/\Omega_e^2 \gg 1$ (for reasons which will be explained subsequently). Most of the previous works deal with fairly low ratios, $\omega_{pe}^2/\Omega_e^2 \sim O(1)$. Here ω_{pe} and Ω_e are defined by $\omega_{pe}^2=4\pi ne^2/m_e$ and $\Omega_e=eB_0/m_ec$, respectively, where n, e, m_e, B_0, and c represent the ambient density, unit electric charge, electron mass, ambient magnetic-field intensity, and the speed of light *in vacuo*, respectively.

The discussion in Ref. 2 was motivated by the study of sporadic solar metric radio bursts. The actual application of the basic results in Ref. 2 to a model problem appropriate for

[a]Permanent address: Instituto de Física, UFRGS, Caixa Postal 15051, 91501-970 Porto Alegre, RS, Brazil.
[b]Electronic mail: yoonp@ipst.umd.edu

solar radio bursts was recently carried out in Ref. 7. For the case of solar metric radio emissions, it is believed that the plasma frequency ω_{pe} is much higher than the electron gyrofrequency Ω_e. Therefore, we are bound to consider the case of high ω_{pe}/Ω_e, which is much higher than what is usually discussed in the literature.[8–22]

In dealing with such a situation, one is confronted with a number of numerical difficulties, including the fact that one has to solve a large number of roots from the Bernstein wave dispersion relation, involving high harmonic range. To deal with high gyroharmonic modes, an approximation scheme has been devised in Ref. 2, in which information on detailed harmonic structures associated with the solution of the dispersion relation is retained only for a few harmonics in the close vicinity of the plasma frequency, while higher and lower harmonics are smoothed out.

To be specific, take the electrostatic Bernstein wave dispersion relation

$$\epsilon = 1 - r \sum_{n=1}^{\infty} a_n (x^2 - n^2)^{-1} = 0, \tag{3}$$

where $r = \omega_{pe}^2/\Omega_e^2$, $x = \omega/\Omega_e$ is the normalized wave angular frequency, $\lambda = k_\perp^2 T_e/m_e\Omega_e^2$, $k_\perp$ is the perpendicular wave vector component, T_e is the electron temperature, $a_n = 2n^2 I_n(\lambda)\, e^{-\lambda}/\lambda$, and $I_n(\lambda)$ is the modified Bessel function of the second kind of order n. Note that Ref. 2 considers fully electromagnetic dispersion relation for waves propagating perpendicular to the ambient magnetic field, since one of the purposes of Ref. 2 is to demonstrate the interconnection between the fast electromagnetic waves and the Bernstein waves. However, the above electrostatic dispersion relation is sufficient if the purpose is just to describe the wave properties of Bernstein waves.[7]

The approximation scheme employed in Ref. 2 amounts to the following treatment of Eq. (3):

$$r^{-1} = -\sum_{n=1}^{N-2} a_n n^{-2} + \sum_{n=N-1}^{N+1} a_n (x^2 - n^2)^{-1} + \sum_{n=N+2}^{\infty} a_n x^{-2}, \tag{4}$$

where N corresponds to the integer value of $r^{1/2} = \omega_{pe}/\Omega_e$. The idea is to assume that $x^2 \ll n^2$ if $x \ll N$, and that $x^2 \gg n^2$ if $x \gg N$, so that the denominator $(x^2 - n^2)^{-1}$ can be replaced by $-n^{-2}$ and x^{-2}, respectively. As shown in Ref. 2, the solution to Eq. (4) correctly describes gyroharmonic modes $x \approx N, N \pm 1$ to a reasonable degree of accuracy, but the detailed information on higher $(x \gg N)$ and lower gyroharmonic structures $(x \ll N)$ is lost.

While such an approximation may be quite adequate for the description of waves whose frequencies lie near the plasma frequency, i.e., $x \approx r^{1/2} \approx N, N \pm 1$, it can lead to erroneous results in the computation of the growth rate, as has been pointed out later in Ref. 7. The reason is the following. Consider the normalized linear growth rate, $\Gamma = \mathrm{Im}\,\omega/\Omega_e$,

$$\Gamma = \sum_{s=-\infty}^{\infty} \int d\mathbf{u}\, K_s(\mathbf{u})\, \delta\left(\gamma - \frac{s}{x}\right) \frac{\partial f_b(\mathbf{u})}{\partial u_\perp}, \tag{5}$$

where $u_\perp$ is the perpendicular component of the normalized momentum vector $\mathbf{u}$, with respect to the magnetic field, and $\gamma = (1 + u^2)^{1/2}$ is the relativisic mass correction factor. The detailed expression for the kernel $K_s(\mathbf{u})$ is given by

$$K_s(\mathbf{u}) = \frac{\pi r}{\partial\epsilon/\partial x} \frac{\alpha}{\lambda} \frac{\gamma^2}{u_\perp} J_s^2(b), \tag{6}$$

where $r = \omega_{pe}^2/\Omega_e^2$ and $\lambda = k_\perp^2 T_e/m_e\Omega_e^2$ as defined before, $\alpha = T_e/m_e c^2$, $b = (\lambda/\alpha)^{1/2} u_\perp$, and $J_s(b)$ is the Bessel function of the first kind of order s. It was noted in Ref. 7 that the growth of a given gyroharmonic mode, say near Nth harmonic

$$\Gamma(x \sim N),$$

is in general determined not necessarily by the harmonic mode number $s = N$ in the Bessel function summation in Eq. (5), but may involve distant neighboring harmonics, $s \neq N$ when u is sufficiently large. As a result, if one ignores the detailed harmonic structures associated with distant neighbors, then one can miss the most important contribution to the wave growth at that harmonic.

The objective of this paper is to discuss a better approximation scheme in order to facilitate the numerical computation for high harmonic numbers and large ratio of plasma to gyro-frequencies, which corrects the shortcoming of the previous method adopted in Ref. 2.

II. BERNSTEIN MODE INSTABILITY

In the present analysis, the electrons are comprised of a thermal background plus an energetic component of the form given by Eq. (2). We assume that the ratio of the beam electrons to the thermal electrons, n_b/n_0, is small. Specifically, we consider this ratio to be 10^{-3} throughout the present study. We assume 200 eV background electron temperature throughout. Other physical parameters which enter the model are the beam kinetic temperature, $T_b = m_e c^2 \alpha_b^2/2$, the pitch-angle spread parameter, δ, the average beam speed $v_b = (c\, u_b)/(1 + u_b^2)^{1/2}$, and the ratio of plasma frequency to electron gyrofrequency, ω_{pe}/Ω_e.

Under certain conditions, relativistic effect may be important for the Bernstein mode dispersion relation.[23–25] However, in the present case such effects on the real part of the dispersion relation are insignificant. Thus we will follow the traditional nonrelativistic approach[5,6] and adopt Eq. (3), whereas relativistic effects are necessary for the discussion of the growth rate [see Eq. (5)].

In order to justify and describe the new approximation scheme to be utilized, we start by presenting a full numerical solution obtained from Eqs. (3) and (5), for $\omega_{pe}/\Omega_e = 20$. Figure 1 presents the full numerical solution of the dispersion equation (3) and the growth rate (5) as a function of $k_\perp \rho_e$, where $\rho_e = (2T_e/m_e\Omega_e^2)^{1/2}$. Other parameters are $T_e = 200$ eV, $T_b = 500$ eV, $\delta = 0.5$, $n_b/n_0 = 10^{-3}$, and $v_b/c = 0.3$. The real frequencies are shown in Fig. 1(a), which are well known, at least in small harmonic number range—e.g., see Refs. 5 and 6. We note that the electrostatic approximation utilized is justified—for the range of $k_\perp \rho_e$ values considered in the calculation, the condition $k^2 c^2 \ll \omega_{pe}^2$ is satis-

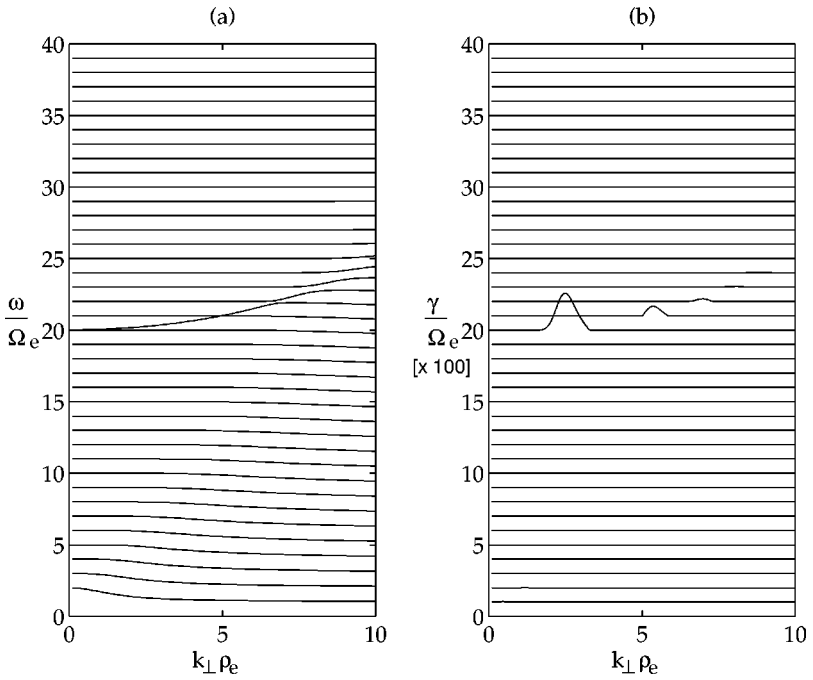

FIG. 1. (a) Bernstein mode dispersion relation for $\omega_{pe}/\Omega_e=20$ and $T_e=200$ eV. (b) Growth rates of Bernstein gyroharmonic waves for $n_b/n_0=10^{-3}$, $v_b/c=0.3$, $T_b=500$ eV, and $\delta=0.5$. The peak growth rate corresponds to $\gamma\sim 5.0\times 10^{-2}\ \Omega_e$.

fied. Figure 1(b) shows the corresponding growth rates, multiplied by a scaling factor of 100. We have not plotted the negative portion of the growth rates. Also, a constant integer n has been added to each value of the growth rate corresponding to an nth mode, in order to avoid superposition in the plot, and to facilitate the one-to-one correspondence between the real frequency and the corresponding growth rate.

From Fig. 1(b), we see that the most unstable mode corresponds to $n=20$, while modes $n=21$ and $n=22$ are progressively less unstable, and the instability virtually disappears in this scale for modes higher than $n=23$. The maximum value of the growth rate occurs for $n=20$, and is seen to be $\gamma_{\max}\simeq 5.0\times 10^{-2}$. We have evaluated the solution of the dispersion relation up to harmonic $n=40$. That is, we have kept $n=1$ to $n=40$ in the summation in Eq. (3). For the evaluation of the growth rate, however, we have kept 50 harmonics in the summation appearing in Eq. (5), i.e., s summation runs from $s=1$ to $s=50$.

We now point out that if one connects the peaks of the bell-shaped Bernstein wave dispersion curves above the plasma frequency, as depicted in Fig. 1(a), the resulting effective dispersion curve can be approximately represented by the dispersion relation of the well-known Langmuir waves in an unmagnetized plasma, i.e.,

$$\omega_r=\omega_{pe}\,(1+3\,k_\perp^2\lambda_{De}^2)^{1/2}, \tag{7}$$

where $\lambda_{De}^2=T_e/(4\pi ne^2)$ is the square of the electron Debye length. The approximation is very good, particularly near the plasma frequency, as shown in Fig. 2(a), where both the exact and the approximate dispersion relations are plotted for the purpose of comparison. In Fig. 2(b), we also present the growth rates, which are calculated on the basis of the two dispersion relations, and multiplied by the same scaling factor of 100.

To further test this aproximation, we consider the case of $\omega_{pe}/\Omega_e=10$ and $v_b/c=0.4$ in Fig. 3, with other parameters as in Figs. 1 and 2, and in the same format. It is seen from Fig. 3(b) that in this case, the mode corresponding to $n=10$ is excited, with maximum growth rate $\gamma\simeq 2.0\times 10^{-2}$. Mode $n=11$ also appears to be unstable, but with a much lower growth rate. It is noteworthy that even for the present case of $\omega_{pe}/\Omega_e=10$, the approximate scheme still provides a reasonably accurate description for the real frequency and the growth rate, although the predicted unstable range of $k_\perp\rho_e$ is narrower than that the exact solution. Note also that the approximate scheme gives a slightly lower value for the maximum growth rate.

The case of $\omega_{pe}/\Omega_e=5$ and $v_b/c=0.5$, with other parameters fixed as in Fig. 1, is shown in Fig. 4. The growth rates, which in this case are multiplied by a factor of 10^3, are shown in Fig. 4(b). Mode $n=5$ is shown to be unstable, with $\gamma_{\max}\simeq 7.0\times 10^{-3}$. Mode $n=6$ also appears to have a small growth rate. The small growth for mode $n=7$ is almost negligible when compared with the other two modes. As the readers can see, the approximate scheme is not accurate for this case, even though it still can be considered useful from a qualitative point of view.

The above results lead us to conclude that the approximate scheme based upon Eq. (7), namely, to replace the Bernstein mode disperison relation by the unmagnetized electrostatic (Langmuir) mode dispersion relation, becomes better as the magnetic field gets weaker, i.e., increasing value of ω_{pe}/Ω_e. Conversely, the scheme becomes progressively inaccurate for decreasing values of ω_{pe}/Ω_e. In this sense, the case $\omega_{pe}/\Omega_e\approx 5$ can be taken as a lower limit for this approximation scheme. In conclusion, for low values of the ratio ω_{pe}/Ω_e, the calculation of the growth rates should use the full dispersion equation.

With the above limitation in mind, we next consider sys-

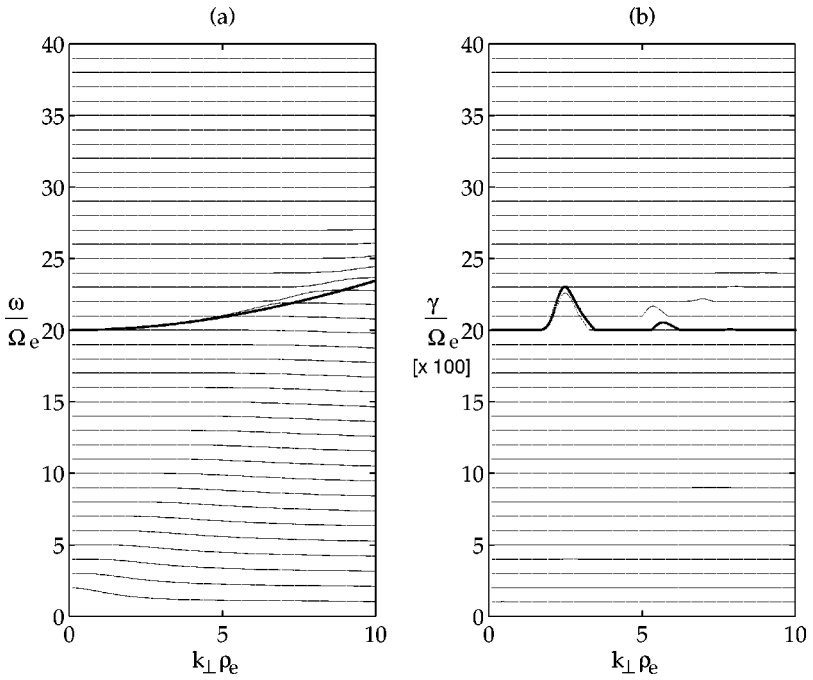

FIG. 2. (a) Comparison of the exact Bernstein mode dispersion relation and the approximate expression (7) for the case considered in Fig. 1. (b) Growth rates computed on the basis of approximate dispersion relation (7) superposed on top of exact results. Thicker lines represent the approximation.

tematic variations of physical parameters. First, in Fig. 5 we consider the case of $\omega_{pe}/\Omega_e=20$ and vary the average beam speed v_b/c from 0.1 through 0.6, while other parameters are fixed as in Fig. 1. In Fig. 5(a) we present the approximate real frequency as prescribed by Eq. (7). In Fig. 5(b) the corresponding growth rates are plotted for each value of v_b/c. In this figure the growth rates are plotted with the multiplicative factor of 2, but to elucidate the detailed features, the constant factor v_b/c is added to each growth rate computed for the same value of v_b/c. It is interesting to observe from Fig. 5(b) that growth rates plotted in $k_\perp\rho_e$ versus v_b/c exhibit repetitive ridge-like structure. Note further that unstable range of parameter v_b/c seems to lie in between $0.15 \leqslant v_b/c \leqslant 0.6$. Finally, a remarkable feature is that excitation of waves at multiple harmonics of the cyclotron frequency is possible for a range of the beam speeds. Take $v_b/c=0.3$ for instance. Maximum excitation occurs for waves with $\omega \simeq 20.2\ \Omega_e$, but a less intense excitation also occurs for $\omega \simeq 21.2\ \Omega_e$. A third peak of excitation may also occur, although with much smaller growth rate.

We now repeat the same calculation as in Fig. 5, but for $\omega_{pe}/\Omega_e=10$. The results are displayed in Fig. 6 in the same format as in Fig. 5. Note that the periodic ridge-like structure in Fig. 6(b) is qualitatively similar to that shown in Fig. 5(b). However, there are some marked differences. For instance, the unstable range of $k_\perp\rho_e$ has become narrower and less

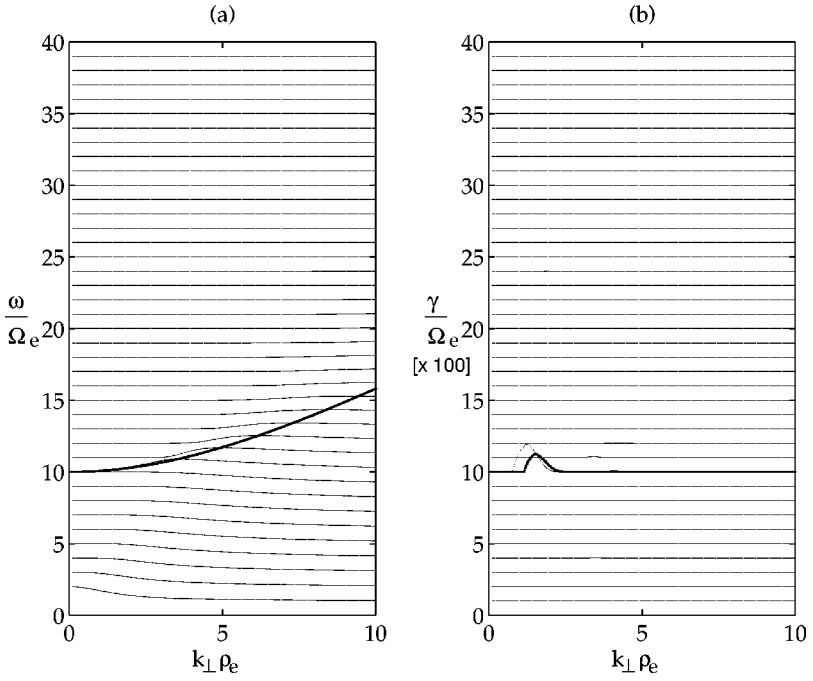

FIG. 3. The same as Fig. 2 except that the case of $\omega_{pe}/\Omega_e=10$ and $v_b/c=0.4$ are considered and compared against the approximate treatment. (a) Real frequency and (b) growth rates. Thicker lines represent the approximation. In this case, the peak growth rate is $\gamma \sim 2.0\times10^{-2}$.

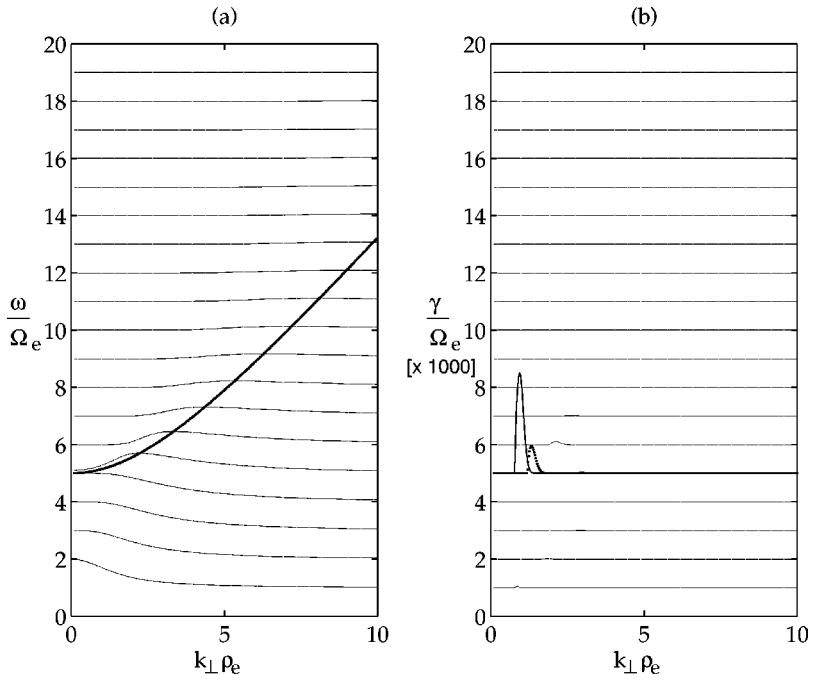

FIG. 4. The same as Fig. 2 except that the case of $\omega_{pe}/\Omega_e=5$ and $v_b/c=0.5$ are considered and compared against the approximate treatment. (a) Real frequency and (b) growth rates. For this case of relatively low frequency ratio, the approximation becomes rather poor. Thicker lines represent the approximation. In this case, the peak growth rate corresponds to $\gamma\sim 7.0\times 10^{-3}$.

extended. Also, instead of 3 to 4 multiple ridges in Fig. 5(b), only a couple of bands are seen in Fig. 6(b).

We continue the computation to the limiting case of $\omega_{pe}/\Omega_e=5$. The results are shown in Fig. 7. The trend that for decreasing values of ω_{pe}/Ω_e the unstable structures move toward higher values of the drift velocity, observed in the cases of $\omega_{pe}/\Omega_e=20$ and $\omega_{pe}/\Omega_e=10$, is also observed here. For this lower density case, however, only one unstable band is observed for the range of beam velocities considered.

In order to shed more light on the parametric dependence of the instability, we show in Fig. 8 the growth rates versus ω_{pe}/Ω_e ranging between 10 and 25, for $v_b/c=0.6$ and other parameters as in Fig. 1. As before, we have enhanced the growth rates by multiplying by a factor of 60. The outcome is a series of unstable bands in the parameter space, $k_\perp\rho_e-\omega_{pe}/\Omega_e$. Note that the waves do not grow in any appreciable manner beyond $k_\perp\rho_e\geqslant 4$, and that the instability disappears for $\omega_{pe}/\Omega_e\geqslant 22$.

The unstable ridges shown in Fig. 8 are largely consistent with the sawtooth-like structures associated with the maximum growth rate plot against ω_{pe}/Ω_e shown in Ref. 2. In that reference, however, the unstable Bernstein waves were shown to be operative for ω_{pe}/Ω_e up to 45 or so. As discussed in the Introduction, the results obtained in Ref. 2 is likely to be erroneous as a result of the incorrect treatment of the problem. In short, the earlier range of the parameter ω_{pe}/Ω_e for which the present Bernstein maser-beam instability is operative appears to have been overestimated.

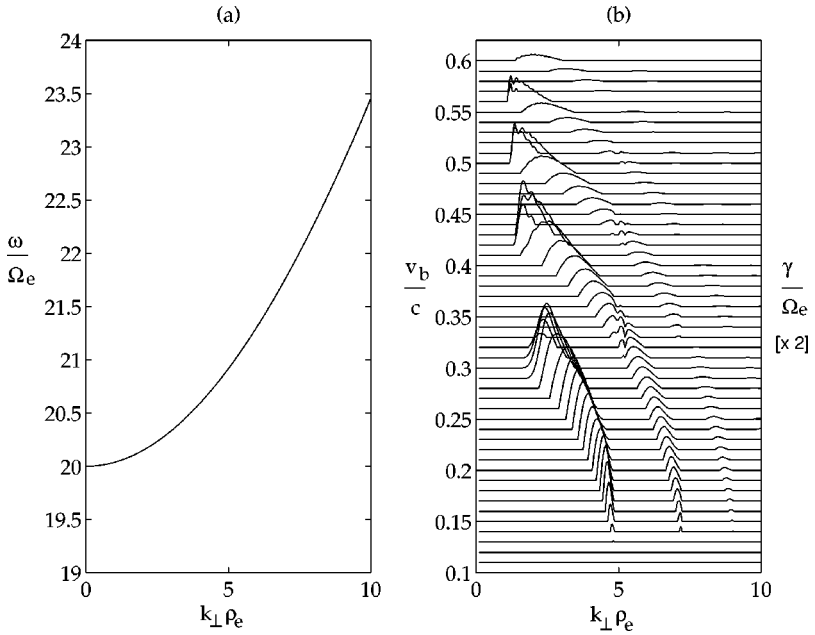

FIG. 5. (a) Real frequency evaluated from Eq. (7), and (b) growth rates versus $k_\perp\rho_e$, for $\omega_{pe}/\Omega_e=20$ and for series of increasing v_b/c, between 0.1 and 0.6. Other parameters as in Fig. 1. The peak growth rate in the plot corresponds to $\gamma\sim 3.2\times 10^{-2}$.

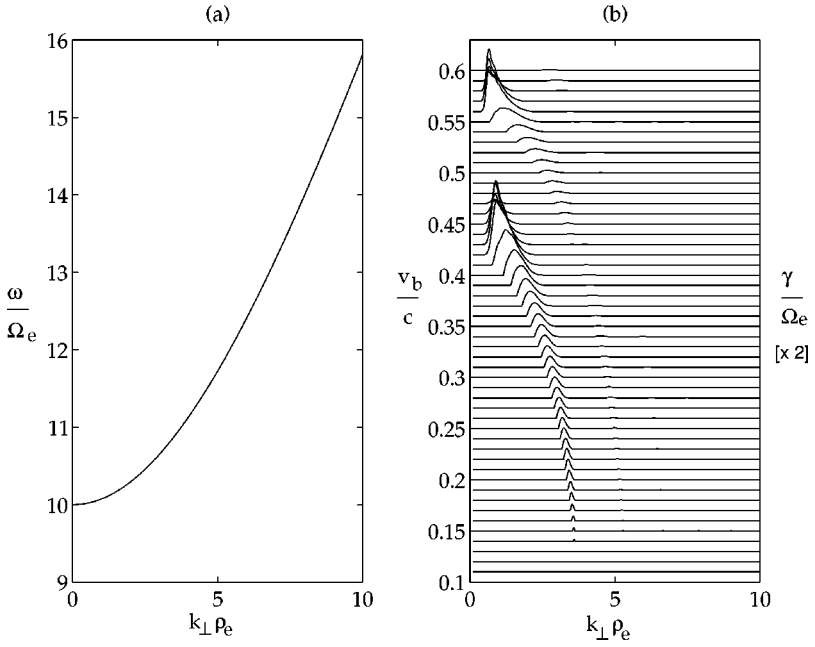

FIG. 6. The same as Fig. 5 except that $\omega_{pe}/\Omega_e=10$ is considered. The peak growth rate is $\gamma\sim 2.7\times 10^{-2}$.

We have repeated the same calculation as in Fig. 8, but for somewhat lower beam speed, namely, $v_b/c=0.2$. The results are plotted in Fig. 9 in the same format as in Fig. 8, except that the growth rates are enhanced by a factor of 30. The results, when compared with Fig. 8, are in overall qualitative agreement. The notable difference is that the range of unstable $k_\perp\rho_e$ appears to be shifted toward higher values, and the unstable range of ω_{pe}/Ω_e also appears to be somewhat broadened. The primary motivation for this analysis regarding the dependence of the instability growth rate on the ratio ω_{pe}/Ω_e is its applicability to the problem of type III radio bursts in the solar corona. Free energy source of the instability is in the stream of fast electrons produced during solar flares. As these electrons travel along open magnetic field lines near the surface of the Sun out toward interplanetary space, they will encounter regions of increasing ω_{pe}/Ω_e. Near the corona, this ratio is estimated to be of the order 10 or so, but near 1 a.u., ω_{pe}/Ω_e can be as high as 50 or even 100. As we have seen, the present analysis shows that the instability ceases to be operative for $\omega_{pe}/\Omega_e\geqslant 22$, which places the limit of applicability of the present mechanism in the context of solar radio bursts.

In Fig. 10, we vary the pitch-angle parameter δ from 0.1 to 2.1, with other parameters as in Fig. 1, except that the beam speed of $v_b/v=0.3$ is chosen. The multiplicative factor of 3 is used in order to enhance the growth rates. As the readers see, the growth rate generally increases in a monotonic fashion as the pitch-angle spread parameter δ increases. We note that δ larger than ~ 2 is unlikely to be realized in actual situations.

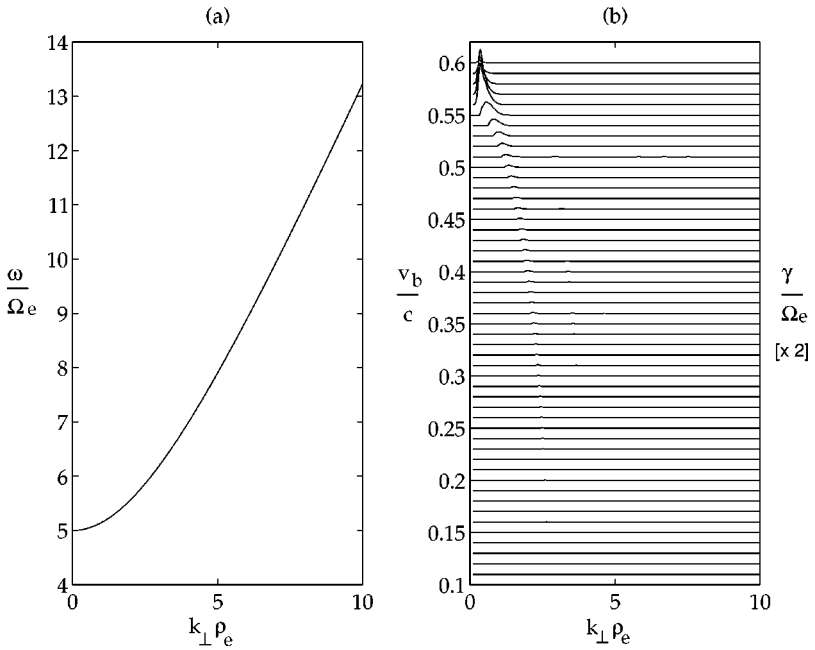

FIG. 7. The same as Fig. 5 except that $\omega_{pe}/\Omega_e=5$ is considered. The peak growth rate in the plot is $\gamma\sim 2.0\times 10^{-2}$.

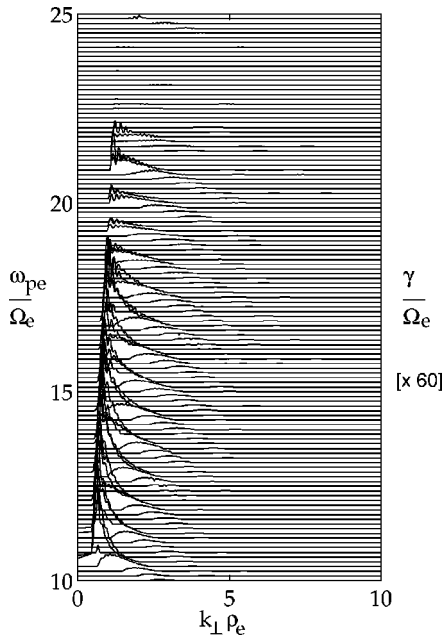

FIG. 8. Growth rates of Bernstein waves computed on the basis of approximation (7) for $v_b/c=0.6$, and ω_{pe}/Ω_e ranging from 10 to 25, with other parameters the same as in Fig. 1. The peak growth rate is $\gamma\sim 4.2\times 10^{-2}$.

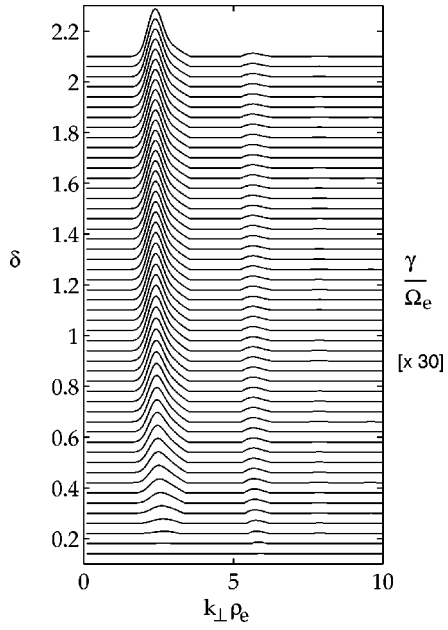

FIG. 10. Growth rates of Bernstein waves computed on the basis of approximation (7) for $v_b/c=0.3$, and δ ranging from 0.1 to 2.1, with other parameters the same as in Fig. 1. The peak growth rate corresponds to $\gamma\sim 6.2\times 10^{-2}$.

In Fig. 11 we show the dependence of the growth rate on the momentum dispersion associated with the beam distribution function, which is modeled by the parameter T_b. Figure 9 is generated for T_b ranging from 200 to 600 eV. Physical parameters are such that $\omega_{pe}/\Omega_e=20$, $v_b/c=0.6$, and other parameters as in Fig. 1. The growth rate for each value of T_b is multiplied by a factor 2×10^3, and the value of the beam temperature is added to it in order to avoid the piling up of curves along one horizontal axis. It is seen that the growth rates increase as the beam temperature is decreased.

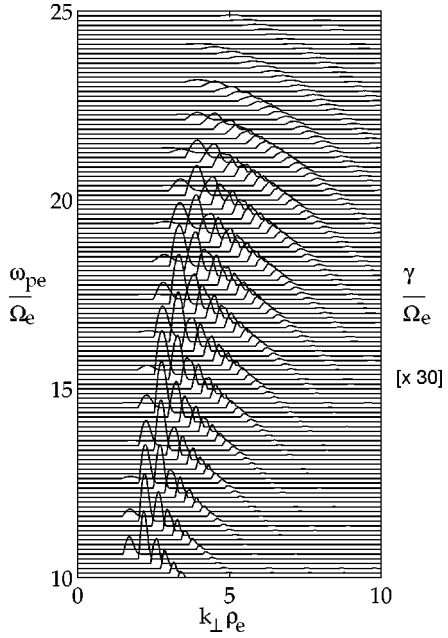

FIG. 9. The same as Fig. 8(a), except that a somewhat lower value of the beam speed, $v_b/c=0.2$ is considered. The peak growth rate is $\gamma\sim 3.0\times 10^{-2}$.

The discussion presented in the preceding discussion is restricted to Bernstein waves propagating in exactly perpendicular directions. At this point it is appropriate to briefly discuss the effects of small but finite $k_\parallel$ on the growth rate. In Fig. 12, we have plotted the growth rates of Bernstein waves versus $k_\perp\rho_e$ and $k_\parallel\rho_e$, for the same set of physical parameters as in Fig. 1, except that $v_b/c=0.3$ and the scaling factor of 0.1 are used. It is seen that the growth rate gradually decreases in magnitude and the range of $k_\perp\rho_e$ as $k_\parallel\rho_e$ increases in the negative direction. On the other hand, for increasing $k_\parallel\rho_e$, both the magnitude and the unstable range of $k_\perp\rho_e$ associated with the present Bernstein growth rate increases.

In Fig. 13, we plot the same growth rate curves as in Fig. 12 with the same set of physical parameters, except that the beam speed corresponding to $v_b/c=0.6$ is adopted, and the scaling factor is unity. As the figure shows, for this case of higher beam speed, the near-perpendicular propagation, $k_\parallel\rho_e\approx 0$ represents the most unstable case, and the mode stabilizes as $k_\parallel\rho_e$ increases in magnitude in both the positive and negative directions. Thus, there appears to be no simple conclusion to discuss the behavior of the present maser instability with a finite and small $k_\parallel$.

III. DISCUSSION AND CONCLUSIONS

In this study we have discussed the instability of thermal extraordinary-mode Bernstein waves excited by energetic electrons which possess a net drift along the ambient magnetic field, and which feature a partial spherical shell-like configuration in momentum space as a result of (presumed) pitch-angle scattering by low-frequency Alfvénic turbulence.

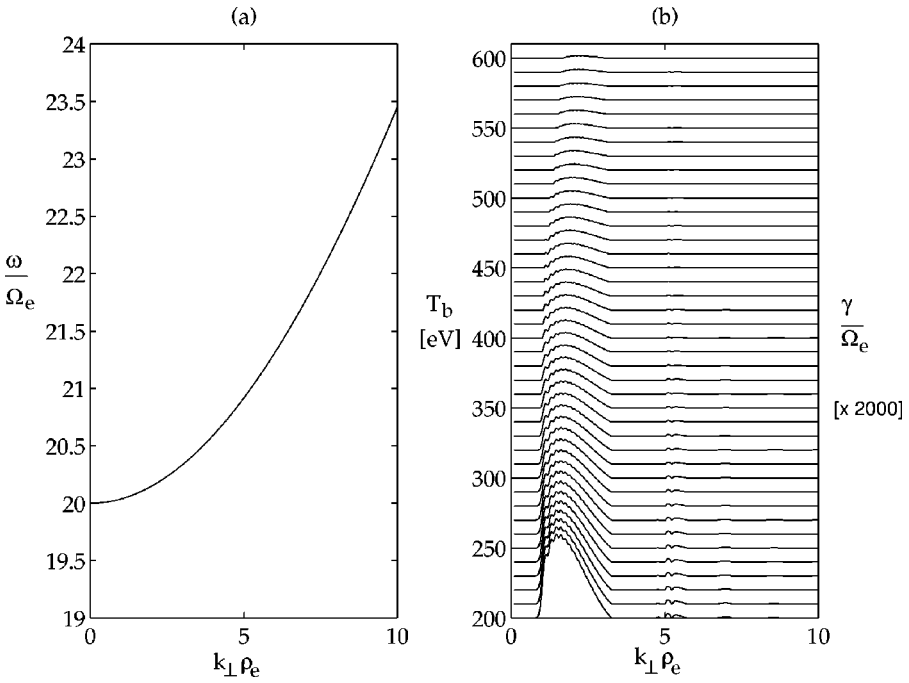

FIG. 11. (a) Real frequency evaluated from Eq. (7), and (b) growth rates versus $k_\perp \rho_e$, for T_b ranging from 200 to 600 eV. Other parameters as in Fig. 1. The peak growth rate corresponds to $\gamma \sim 3.0\times 10^{-2}$.

The instability operates on generalized Bernstein harmonic modes with characteristic $k_\perp \rho_e$ of order unity or higher.

We have paid special attention to situations where the ratio ω_{pe}/Ω_e is relatively high, since the motivation for the present work stems from the application in the solar and interplanetary radio emission process. For such an application the ratio ω_{pe}/Ω_e is of the order 10 or so near the corona and can be as high as 50 or even 100 near 1 a.u. The traditional explanation for solar metric radio bursts relies on nonlinear conversion of Langmuir waves, excited by a beam of electrons, into transverse electromagnetic waves.[26,27] The instability which we have discussed in this paper is also driven by a beam of electrons, but the two instabilities are very distinct from each other. While the present instability excites near-perpendicular wave modes, the usual bump-on-tail instability predominantly excites electrostatic wave propagating nearly parallel to the ambient magnetic field.

Note that, for all cases considered, the excited modes are located above the plasma frequency, and have positive derivatives regarding the parameter $k_\perp \rho_e$. Therefore these excited waves can be converted to the fast *X*-mode, provided that the ratio ω_{pe}/Ω_e increases adiabatically as the wave propagates away from its source. As we have already pointed

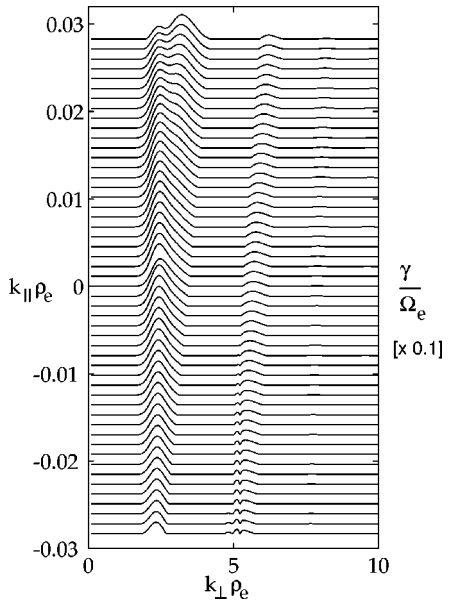

FIG. 12. Growth rates of Bernstein waves against $k_\perp \rho_e$ and small but finite parallel wave vector component, $k_\parallel \rho_e$, for the same set of parameters as in Fig. 1, except that $v_b/c = 0.3$. The peak growth rate corresponds to $\gamma \sim 3.0\times 10^{-2}$.

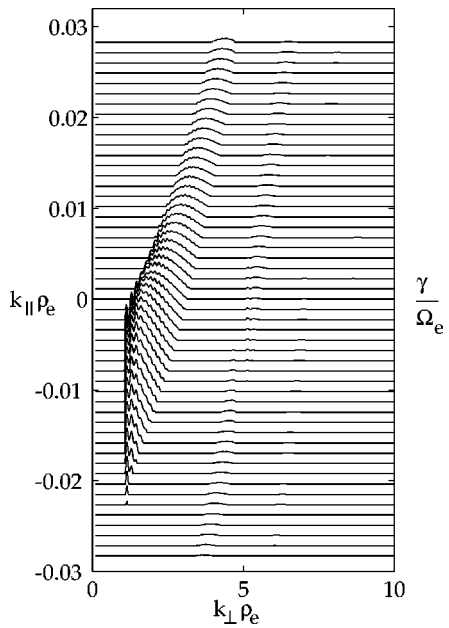

FIG. 13. The same as in the previous figure, except that the beam speed $v_b/c = 0.6$ is adopted. The peak growth rate corresponds to $\gamma \sim 5.0\times 10^{-3}$.

out in a previous work,[7] these thermal extraordinary Bernstein modes excited above electron plasma frequency may suffer mode conversion to escaping radiation, if they travel toward the region of increasing magnetic field and plasma density (toward the Sun).[2]

ACKNOWLEDGMENTS

The present research was supported by grant ATM 9802498 from the National Science Foundation and by Grant No. DE-FG02-00ER54584 from the U.S. Department of Energy. L.F.Z. thanks partial support from Brazilian agencies CAPES and CNPq.

[1]N. A. Krall and A. W. Trivelpiece, *Principles of Plasma Physics* (McGraw-Hill, New York, 1973).
[2]P. H. Yoon, C. S. Wu, and Y. Li, J. Geophys. Res. **104**, 19801 (1999).
[3]I. B. Bernstein, Phys. Rev. **109**, 10 (1958).
[4]T. H. Stix, *The Theory of Plasma Waves* (McGraw-Hill, New York, 1962).
[5]S. Puri, F. Leuterer, and M. Tutter, J. Plasma Phys. **9**, 89 (1973).
[6]S. Puri, F. Leuterer, and M. Tutter, J. Plasma Phys. **14**, 169 (1975).
[7]C. S. Wu, P. H. Yoon, and Y. Li, Astrophys. J. **540**, 572 (2000).
[8]F. W. Crawford, R. S. Harp, and T. D. Mantei, J. Geophys. Res. **72**, 57 (1967).
[9]R. W. Fredericks, J. Geophys. Res. **76**, 5344 (1971).
[10]T. S. T. Young, J. D. Callen, and J. E. McCune, J. Geophys. Res. **78**, 1082 (1973).
[11]V. I. Karpman, J. K. Alekhin, N. D. Borisov, and N. A. Rjabova, Plasma Phys. **17**, 361 (1975).
[12]V. V. Zheleznyakov and E. Y. Zlotnik, Sol. Phys. **43**, 431 (1975).
[13]M. Ashour-Adballa and C. F. Kennel, J. Geophys. Res. **83**, 1531 (1978).
[14]R. F. Hubbard and T. J. Birmingham, J. Geophys. Res. **83**, 4837 (1978).
[15]D. D. Sentman, J. Geophys. Res. **87**, 1455 (1982).
[16]R. M. Winglee and G. A. Dulk, Astrophys. J. **307**, 808 (1986).
[17]R. M. Winglee and G. A. Dulk, Astrophys. J. **310**, 432 (1986).
[18]P. A. Robinson, Sol. Phys. **134**, 299 (1991).
[19]G. D. Fleishman and G. Yastrebov, Sol. Phys. **154**, 361 (1994).
[20]A. J. Willes and P. A. Robinson, Astrophys. J. **467**, 465 (1996).
[21]A. J. Willes and P. A. Robinson, J. Plasma Phys. **58**, 171 (1997).
[22]V. G. Ledenev, Sol. Phys. **179**, 405 (1998).
[23]Yu. N. Dnestrovskii, D. P. Kostomarov, and N. V. Skrydlov, Sov. Phys. Tech. Phys. **8**, 691 (1964).
[24]P. A. Robinson, J. Plasma Phys. **37**, 449 (1987).
[25]P. A. Robinson, Phys. Fluids **31**, 107 (1988).
[26]V. L. Ginzburg and V. V. Zheleznyakov, Sov. Astron. **2**, 653 (1958).
[27]D. B. Melrose, in *Solar Radiophysics* (Cambridge University Press, New York, 1985), p. 177.